Tbit/s switching scheme for ATM/WDM networks

J. Nir, I. Elhanany and D. Sadot

A new high capacity, reservation-based switch architecture for ATM/WDM networks is presented. The scheme is contention-free and highly flexible yielding a powerful solution for high-speed broadband packet-switched networks. Switching management and control are studied for data rates of up to 10Gbit/s/port, providing and aggregated throughput of over 1Tbit/s.

Introduction: Wavelength division multiplexing (WDM) is widely recognised as a promising technology for high-capacity, scalable, cost effective optical networks. Considerable attention has been paid to WDM contention resolution and wavelength assignment issues, commonly targeted at packet-switched networks such as asynchronous transfer mode (ATM) [1, 2]. Recently, several switching schemes were designed in order to support high capacity, large number of ports and low latency requirements [2 – 4]. Here, we introduce a new WDM packet-switching scheme that offers Tbit/s capacity along with support of over 128 ports and switching latency of up to tens of microseconds. The new architecture is contention-free and has the advantages of low implementation complexity and high scalability. In addition, the architecture can easily be adapted to comply with diverse quality of service (QoS) demands.

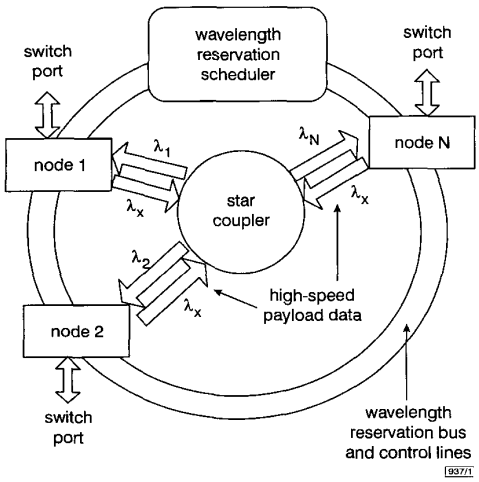

Fig. 1 *Tbit/s ATM over WDM switch architecture*

Switching architecture: Fig. 1 depicts the proposed switch architecture. The nodes, corresponding to the switch ports, have bi-directional optical data links interconnected via an optical passive star coupler. Each transmitter can be tuned to any of the N wavelengths, while each receiver is assigned a fixed and distinct wavelength. ATM traffic received at each port is distributed to different buffers within the node on a cell-by-cell basis, where each buffer relates to a single wavelength according to the desired destination node. All nodes are connected to a central wavelength reservation scheduler via a common electronic wavelength reservation bus, and individual control lines. The N bus lines are accessible to all nodes and indicate the reservation status of each of the N wavelengths. The individual control lines are used by the scheduler to signal each node, in turn, to commence the wavelength reservation procedure.

Wavelength reservation: On receiving a control signal from the wavelength reservation scheduler, each node performs wavelength reservation according to two major guidelines: global switch resources status, i.e. available wavelengths at the reservation time, and local considerations, i.e. the status and priorities of the node's internal buffers. Fig. 2 illustrates a block diagram of the wavelength reservation hardware of a node in an 8×8 switch. At the highest level, the wavelength reservation status lines, denoted by S_i, either grant or discard buffer priorities, denoted by P_i, via designated AND logic. Consequently, only buffer indices, denoted by I_i, relating to available wavelengths advance to the lower levels. Each level consists of a set of comparators, which receive as input a pair of indices along with their respective priorities and output the higher priority and its corresponding index. The output of the last comparator determines the 'prevailing' buffer, which held the highest priority out of the subset of buffers relating to unreserved wavelengths. Any number of parameters, such as buffer load, accumulated delay and required QoS can affect the buffer priority metrics. Node wavelength selection is instantly followed by assertion of the relevant line within the wavelength reservation bus. At that point, utilising a weighted Round Robin procedure, the central scheduler signals the next node to begin wavelength reservation. Contention is avoided, since at any given time only one node attempts to reserve a wavelength. After all N nodes complete wavelength reservation, high-speed data are optically transmitted via the star coupler.

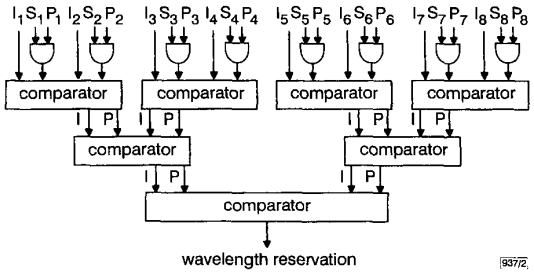

Fig. 2 *Node wavelength reservation scheme block diagram for 8 × 8 switch*

The wavelength reservation and data transmission are conducted in a time slot discipline. Nodes transmit data concurrently at wavelengths reserved during the previous time slot. Assuming N nodes, the time slot period can be calculated as $t_{ts} = N \cdot \log_2(N) \cdot t_c$, where t_c is the processing time for a single comparator. Accordingly, t_{ts} dictates the minimal number of cells required to be transmitted during each time slot and hence the queueing time delays.

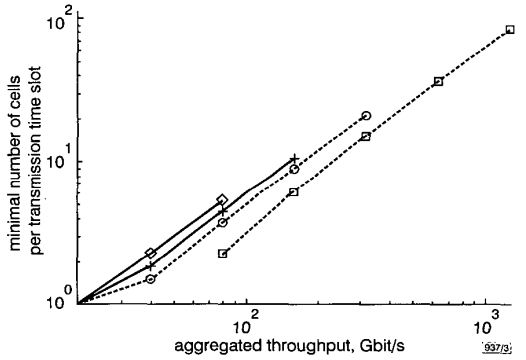

Fig. 3 *Switch aggregated throughput for different port bit rates*

◇ 622Mbit/s (OC-12)
+ 1.24Gbit/s (OC-24)
○ 2.48 Gbit/s (OC-48)
□ 9.95Gbit/s (OC-192)

Simulation results: Taking into consideration present VLSI technology, t_c = 4ns was found feasible. As a result, extremely short processing time for resource allocation is attained, yielding high switching performance. Fig. 3 presents the number of cells required to be transmitted during each time slot under heavy traffic conditions, against switch aggregated throughput. Various port bit rates are presented as a parameter. The marks on each curve represent standard numbers of ports, e.g. 8, 16, 32, 64 and 128. Simulations demonstrate that Tbit/s switching capacity at 9.95Gbit/s (OC-192) per port can be achieved. Up to 128 ports are supported with only 63 cells transmitted per time slot, and with a total required buffer size of a few hundreds of cells. This can be compared to other high-speed buffer management approaches such as in [1]. In such architectures, buffer selection is executed using reservation-free Round-Robin algorithms that attempt to

minimise the processing time. Contention is avoided by applying multilayered buffer configurations and backpressure mechanisms, which limit performance and scalability.

Although in this Letter we discuss fixed-size packets, this method can be applied to variable-size packets, e.g. IP traffic. By the same token, optical WDM can be replaced by other multiplexing technology, e.g. optical SDM (space division multiplexing).

Conclusions: A novel Tbit/s switch architecture for ATM over WDM packet-switched networks has been proposed. By applying an ultra-high speed scheduling discipline, extremely high capacity and low latency switching are achieved for fabrics of up to 128 × 128. The design is simple, scalable and flexible to support diverse traffic characteristics. The method can be adapted to IP traffic and to various multiplexing technologies.

Acknowledgment: This work was supported by the Israeli Ministry of Science under contract no. 9404-1-97, the Wolfson foundation and the Rector's office at the Ben-Gurion University of the Negev.

28 September 1998
Electronics Letters Online No: 19990004

J. Nir, I. Elhanany and D. Sadot (*Electrical and Computers Engineering Department, Ben-Gurion University, Beer-Sheva 84105, Israel*)

E-mail: sadot@ee.bgu.ac.il

References

1 CHIUSSI, F.M., KNEUER, J.G., and KUMAR, V.P.: 'Low-cost scalable switching solutions for broadband networking: The ATLANTA architecture and chipset', *IEEE Commun. Mag.*, 1997, **25**, (12), pp. 44–53

2 MCKINNON, M.W., ROUSKAS, G.N., and PERROS, H.G.: 'Performance analysis of single hop photonic ATM switch architecture with tunable transmitters and fixed frequency receivers', *Performance evaluation*, 1998, **33**, (2), pp. 113–136

3 SIVARAMAN, V., and ROUSKAS, G.N.: 'HiPeR-1: A high performance reservation protocol with look-ahead for broadcast WDM networks'. Proc. IEEE INFOCOM '97, April 1997, Vol. 3, pp. 1270–1277

4 SALISBURY, C., and MELHEM, R.: 'A high speed scheduler/controller for unbuffered Banyan networks'. Proc. IEEE ICC'98, Atlanta, GA, June 1998 (Session S18-6)

Electromagnetic penetration into 2D multiple slotted rectangular cavity: TE-wave

H.H. Park and H.J. Eom

Electromagnetic wave penetration into a two-dimensional rectangular cavity with multiple slots in an infinite conducting plane with a finite thickness is investigated. The Fourier transform and a mode-matching technique are used to obtain simultaneous equations, which are solved to represent the scattered and penetrated fields in series forms suitable for numerical computations.

Introduction: Electromagnetic penetration into a cavity with a slot has been of importance in EMI/EMC-related problems and in the area of target indentification [1, 2]. In this Letter, the Fourier transform and the mode-matching technique as used in [3] are developed for studying the resonance behaviours of the electric and the magnetic fields inside a 2D rectangular cavity excited through multiple slots by a TE-polarised plane wave where the magnetic field vector of the incident wave is parallel to the axis of the shell. The solution is a fast-converging series form, which is numerically efficient. The numerical implementations are taken to illustrate the resonance behaviours of the internal cavity in terms of the size of the cavity and the slot and the penetration effects due to the multiple slots.

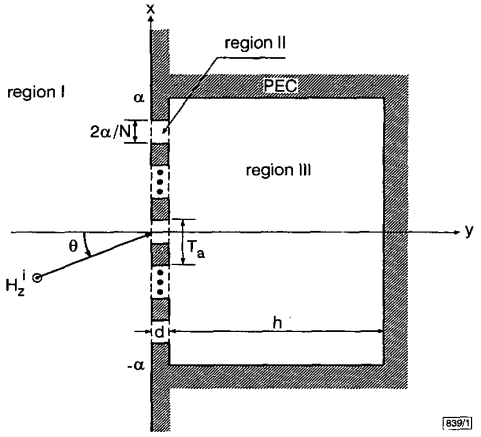

Fig. 1 *Geometry of 2D multiple slotted rectangular cavity: TE-wave*
N = number of slots

Field representation and boundary conditions: An electromagnetic wave with TE-polarisation is obliquely incident on a multiple slotted rectangular cavity as shown in Fig. 1. In region I, the incident and reflected H-fields are

$$\bar{H}^i(x,y) = -\hat{z}e^{ik_x x + ik_y y} \tag{1}$$

$$\bar{H}^r(x,y) = -\hat{z}e^{ik_x x - ik_y y} \tag{2}$$

where $k_x = k_0 \sin\theta$, $k_y = k_0 \cos\theta$, and $k_0 = \omega\sqrt{(\mu_0\epsilon_0)} = 2\pi/\lambda$ is the free space wavenumber. The scattered H_z^s-field in region I is given by

$$H_z^s(x,y) = \frac{1}{2\pi}\int_{-\infty}^{\infty} \tilde{H}_z^s(\zeta)e^{-i\zeta x + i\kappa y}d\zeta \tag{3}$$

where $\kappa = \sqrt{(k_0^2 - \zeta^2)}$. Assume $\tilde{H}_z^s(\zeta)$ is the Fourier transform of $H_z^s(x, 0)$ given by $\tilde{H}_z^s(\zeta) = \int_{-\infty}^{\infty} H_z^s(x, 0)e^{i\zeta x}dx$.

In region II ($|x - lT_a| < a$, $0 < y < d$) the magnetic field $H_z^{II}(x, y)$ inside the slot is

$$H_z^{II}(x,y) = \sum_{m=0}^{\infty}\left[\bar{c}_m^l \cos\xi_m(y-d) + \bar{d}_m^l \sin\xi_m(y-d)\right] \times \cos a_m(x - lT_a + a) \tag{4}$$

where $a_m = m\pi/(2a)$ and $\xi m = \sqrt{(k_0^2 - a_m^2)}$.

In region III ($|x| < \alpha$, $d < y < d + h$) the magnetic field $H_z^{III}(x, y)$ is

$$H_z^{III}(x,y) = \sum_{n=0}^{\infty}\bar{e}_n \cos\gamma_n(y-d-h)\cos\alpha_n(x+\alpha) \tag{5}$$

where $\alpha_n = n\pi/(2\alpha)$ and $\gamma_n = \sqrt{(k_0^2 - \alpha_n^2)}$.

To determine the unknown coefficients $\bar{c}_m^l$ and $\bar{d}_m^l$, we enforce the boundary conditions on E_x and H_z at $y = 0$ and d. First, we apply the boundary conditions on E_x and H_z at $y = 0$.

$$E_x^i(x,0) + E_x^r(x,0) + E_x^s(x,0) = \begin{cases} E_x^{II}(x,0) & \text{for } |x - lT_a| < a \\ 0 & \text{elsewhere} \end{cases} \tag{6}$$

and

$$H_z^i(x,0) + H_z^r(x,0) + H_z^s(x,0) = H_z^{II}(x,0) \quad \text{for } |x - lT_a| < a \tag{7}$$

Applying the Fourier transform to eqn. 6 and solving for $\tilde{H}_z^s(\zeta)$, and then substituting $\tilde{H}_z^s(\zeta)$ into eqn. 7, multiplying eqn. 7 by $\cos a_p(x - rT_a + a)$ and performing integration from $rT_a - a$ to $rT_a + a$, we obtain the simultaneous equation for $\bar{c}_m^l$ and $\bar{d}_m^l$:

$$2ai k_x F_p(k_x a)e^{ik_x rT_a} - \frac{ia^3}{2\pi}\sum_{l=-L_1}^{L_2}\sum_{m=0}^{\infty}\xi_m\left[\bar{c}_m^l \sin(\xi_m d) + \bar{d}_m^l \cos(\xi_m d)\right]\bar{I}_{mp}^{lr} = \varepsilon_p\left[\bar{c}_p^r \cos(\xi_p d) - \bar{d}_p^r \sin(\xi_p d)\right]\delta_{mp}\delta_{lr} \quad p = 0, 1, 2, \ldots \tag{8}$$